

## Communication

### A new approach to materials discovery for electronic and thermoelectric properties of single-molecule junctions

David Zsolt Manrique, Qusiy Hibbeb Al-Galiby, Wenjing Hong, and Colin J. Lambert

*Nano Lett.*, **Just Accepted Manuscript** • Publication Date (Web): 19 Jan 2016

Downloaded from <http://pubs.acs.org> on January 19, 2016

#### Just Accepted

“Just Accepted” manuscripts have been peer-reviewed and accepted for publication. They are posted online prior to technical editing, formatting for publication and author proofing. The American Chemical Society provides “Just Accepted” as a free service to the research community to expedite the dissemination of scientific material as soon as possible after acceptance. “Just Accepted” manuscripts appear in full in PDF format accompanied by an HTML abstract. “Just Accepted” manuscripts have been fully peer reviewed, but should not be considered the official version of record. They are accessible to all readers and citable by the Digital Object Identifier (DOI®). “Just Accepted” is an optional service offered to authors. Therefore, the “Just Accepted” Web site may not include all articles that will be published in the journal. After a manuscript is technically edited and formatted, it will be removed from the “Just Accepted” Web site and published as an ASAP article. Note that technical editing may introduce minor changes to the manuscript text and/or graphics which could affect content, and all legal disclaimers and ethical guidelines that apply to the journal pertain. ACS cannot be held responsible for errors or consequences arising from the use of information contained in these “Just Accepted” manuscripts.



ACS Publications

1  
2  
3  
4  
5  
6  
7  
8  
9  
10  
11  
12  
13  
14  
15  
16  
17  
18  
19  
20  
21  
22  
23  
24  
25  
26  
27  
28  
29  
30  
31  
32  
33  
34  
35  
36  
37  
38  
39  
40  
41  
42  
43  
44  
45  
46  
47  
48  
49  
50  
51  
52  
53  
54  
55  
56  
57  
58  
59  
60

# A new approach to materials discovery for electronic and thermoelectric properties of single- molecule junctions

*David Zsolt Manrique<sup>†,\*</sup>, Qusiy Al-Galiby<sup>†</sup>, Wenjing Hong<sup>‡,§</sup>, Colin J. Lambert<sup>†</sup>*

<sup>†</sup> Department of Physics, Lancaster University, Lancaster LA1 4YB, United Kingdom

<sup>‡</sup> Department of Chemical and Biochemical Engineering, College of Chemistry and Chemical  
Engineering, Xiamen University, Xiamen 361005, China

<sup>§</sup> Department of Chemistry and Biochemistry, University of Bern, Freiestrasse 3, CH-3012  
Bern, Switzerland

KEYWORDS. Single molecular junction, quantum circuit, thermopower, conductance,  
asymmetric and symmetric junctions, thermoelectricity

ABSTRACT. We have investigated a large set of symmetric and asymmetric molecules to  
demonstrate a general rule for molecular-scale quantum transport, which provides a new  
route to materials design and discovery. The rule states “the conductance  $G_{\text{XBY}}$  of an  
asymmetric molecule is the geometric mean of the conductance of the two symmetric  
molecules derived from it and the thermopower  $S_{\text{XBY}}$  of the asymmetric molecule is the  
algebraic mean of their thermopowers”. The studied molecules have a structure X-B-Y,  
where B is the backbone of the molecule, while X and Y are anchor groups, which bind the  
molecule to metallic electrodes. When applied to experimentally-measured histograms of

1  
2  
3 conductance and thermopower, the rules apply to the statistically-most-probable values. We  
4 investigated molecules with anchors chosen from the following family: cyano, pyridl,  
5 dihydrobenzothiol, amine and thiol. For the backbones B, we tested fourteen different  
6 structures. We found that the formulae  $(G_{XBY})^2 = G_{XBX} * G_{YBY}$  and  $S_{XBY} = (S_{XBX} + S_{YBY}) / 2$  were  
7 satisfied in the large majority of the cases, provided the Fermi energy is located within the  
8 HOMO-LUMO gap of the molecules. The circuit rules imply that if measurements are  
9 performed on molecules with  $n_A$  different anchors and  $n_B$  different backbones, then properties  
10 of  $n_A(n_A+1)n_B/2$  molecules can be predicted. So for example, in the case of 20 backbones  
11 and 10 anchors, 30 measurements (or reliable calculations) can provide a near quantitative  
12 estimate for 1070 measurements of other molecules, no extra cost.  
13  
14  
15  
16  
17  
18  
19  
20  
21  
22  
23  
24  
25

26 Nowadays there exist a variety of techniques for measuring the electrical conductance  $G$  and  
27 thermopower  $S$  of single molecules, such as scanning tunneling microscopy (STM)<sup>1,2</sup>, current  
28 probe atomic force microscopy<sup>3, 4</sup>, STM-break junction (STM-BJ)<sup>5-7</sup>, crossed-wire  
29 geometry<sup>8</sup>, nanoparticle junctions<sup>9, 10</sup>, mechanically controlled break junctions(MCBJ)<sup>11</sup>,  
30 electromigration setups<sup>12,13</sup> and nanopores<sup>14</sup>. Schematically, the measured systems are of the  
31 form electrode-X-B-Y-electrode, where X and Y are anchor groups, which bind the molecule  
32 to the electrodes and B is the functional backbone of the molecule. A number of experimental  
33 and theoretical studies demonstrated that useful electronic and thermoelectric functionalities,  
34 such as switching, sensing, rectifying and heat-to-electricity converters can be optimised by  
35 modifying the backbone B of the molecules, as well as the anchors<sup>15-18</sup>. For molecules of  
36 length less than approximately 3 nm, charge transport has been shown to be dominated by  
37 phase coherent electron transport<sup>19</sup>, and therefore the subparts X, B and Y cannot be assigned  
38 their own conductance or thermopower within the molecule. Nevertheless a recent  
39 experimental and theoretical study demonstrated that for molecules containing serially  
40 connected meta, para or ortho phenyl rings, their conductances obtained by changing the  
41  
42  
43  
44  
45  
46  
47  
48  
49  
50  
51  
52  
53  
54  
55  
56  
57  
58  
59  
60

sequencing of the rings are related to each other<sup>20</sup>, which implies that molecular subparts X, B and Y are individually characterizable by single numbers. These ‘circuit rules’ provide a theoretical basis for the systematic categorisation of trends in single-molecule measurement data. They provide guidance for the design and synthesis of molecular devices with optimal electronic and thermoelectric properties by treating molecular components as individual building blocks. In this letter we show that this rule is much more widely applicable than initially suggested in ref.<sup>20</sup> and can be applied to a very wide range of symmetric and asymmetric molecules, with or without donor and/or acceptor groups. For the first time we also provide a circuit rule for the thermopower  $S$  (i.e. Seebeck coefficient) of single molecules. These circuit rules are of interest, because they provide rules for the discovery of new materials by predicting electronic and thermoelectric properties of molecules. This is particularly important, because theoretical methods such as density functional theory and GW many body theory do not usually provide quantitative predictions of such properties<sup>21</sup>.

It is well known that the transmission coefficient of two serially-connected phase-coherent scatterers with individual transmission coefficients  $T_1$  and  $T_2$ , is of the form  $T = \frac{T_1 T_2}{1 - 2\sqrt{R_1 R_2} \cos \varphi + R_1 R_2}$ , where  $\varphi$  is a quantum phase arising from quantum interference (QI) between the scatterers<sup>22</sup>. Consequently the transmission coefficient  $T$  cannot normally be factorized to a product of terms associated with the individual scatterers alone. Nevertheless, the following argument leads us to a ‘circuit rule’ which describes how the transmission changes when the sequential order of the scatterers is changed. First we note that Dyson’s equation for the Green’s function of a structure comprising three serially-connected subsystems X, B, Y is of the form

$$\begin{bmatrix} E - H_X & -V_X & 0 \\ -V_X^\dagger & E - H_B & -V_Y \\ 0 & -V_Y^\dagger & E - H_Y \end{bmatrix} \begin{bmatrix} G_{XX} & G_{XB} & G_{XY} \\ G_{BX} & G_{BB} & G_{BY} \\ G_{YX} & G_{YB} & G_{YY} \end{bmatrix} = I,$$

where  $H_X$  ( $H_Y$ ) is the Hamiltonian of the combined left electrode and anchor X (right electrode and anchor Y) and  $V_X$  ( $V_Y$ ) is the coupling between the backbone of the molecule and the anchor X (Y). From this expression, the relevant sub-matrix of the Green's function that describes electron propagation across the molecule from X to Y is

$$G_{YX} = g_Y V_Y^\dagger G_{BB} V_X^\dagger g_X \quad (1)$$

where  $G_{BB} = (E - H_B - \Sigma)^{-1}$  is the Green's function of the coupled backbone and  $g_X$  ( $g_Y$ ) is the Green's function of the combined left electrode and anchor X (right electrode and anchor Y) and  $\Sigma = V_X g_X V_X^\dagger + V_Y^\dagger g_Y V_Y$ . If the electrodes are coupled to the anchors through a single site at both ends, the transmission coefficient through the molecule from one electrode to the other is  $T_{XBY} = (\hbar v)^2 |G_{YX}|_{ij}^2$ , where  $v$  is the group velocity of the electrodes,  $i$  and  $j$  denote the anchor sites connected to electrodes<sup>21,23</sup>. For molecules such as those shown in figure 1, the anchors are linked to only single sites  $k, l$  in the backbone, in which case the transmission coefficients takes the form

$$T_{XBY} = \hbar v \left| [g_Y V_Y^\dagger]_{ik} \right|^2 \left| [G_{BB}]_{kl} \right|^2 \hbar v \left| [V_X^\dagger g_X]_{lj} \right|^2 = A_Y \times B_B \times A_X, \quad (2)$$

where  $A_X = \hbar v \left| [V_X^\dagger g_X]_{lj} \right|^2$ ,  $A_Y = \hbar v \left| [g_Y V_Y^\dagger]_{ik} \right|^2$  and  $B_B = \left| [G_{BB}]_{kl} \right|^2$ . The factor  $B_B$  depends on X and Y via the self-energies  $V_X g_X V_X^\dagger$  and  $V_Y^\dagger g_Y V_Y$ . However if the couplings are sufficiently weak and the Fermi energy does not coincide with the poles of  $g_X$  and  $g_Y$ , then  $\Sigma$  can be negligible<sup>21</sup> and from eq. (2) it follows that

$$T_{XBY}^2 = T_{XBX} T_{YBY} \quad (3)$$

The dependency of  $B_B$  of X and Y is the smallest when the Fermi energy is located far away from the poles of  $g_X$  and  $g_Y$ , which is the case for off-resonant electron transport in the co-

1  
2  
3 tunneling regime. Based on the Landauer formula, and since eq. (3) is valid for a range of  
4  
5 energies larger than  $kT=25$  meV, the room temperature conductance also satisfies  
6  
7

$$8 \quad G_{XBY}^2 = G_{XBX}G_{YBY} \quad (4)$$

9  
10  
11 Since this approximate relation is true for a range of energies within the HOMO-LUMO gap,  
12  
13 the rules for the derivatives of the logarithm of the transmission coefficients are expected to  
14  
15 satisfy  $\frac{d}{dE} \log T_{XBY}^2 = \frac{d}{dE} \log T_{XBX} + \frac{d}{dE} \log T_{YBY}$ , which leads the circuit rule for the low-  
16  
17 temperature thermopower<sup>24</sup>:  
18  
19

$$20 \quad 2S_{XBY} = S_{XBX} + S_{YBY} \quad (5)$$

21  
22  
23 Although density functional theory (DFT) is not a quantitative theory, it has been shown to  
24  
25 correctly predict trends in transport properties. In order to demonstrate that the above rules  
26  
27 are valid for a wide range of molecular junctions, we performed DFT-based electron transport  
28  
29 calculations for 193 molecules. The molecules are classified according to their backbone  
30  
31 structures, and their attached anchors (as shown in Figure 1a,b,c). In Figure 1, X and Y  
32  
33 indicates the location of the anchor groups. The anchor groups X and Y are chosen from the  
34  
35 family CN, Py, BT, NH<sub>2</sub>, S, several of which have been studied extensively in the literature<sup>25-</sup>  
36  
37 <sup>32</sup>. In Figure 1a, shows 180 molecules formed from 12 backbones and five anchor groups. In  
38  
39 the case of the 10 X-R-Y molecules shown in Figure 1b, X and Y are chosen to be one of  
40  
41 CN, PY, NH<sub>2</sub>, S and in the case of the 3 X-But-Y molecules shown in Figure 1c, X and Y are  
42  
43 chosen to be either S or NH<sub>2</sub>. Figure 1a,b illustrates the anchor as well as the aromatic rings,  
44  
45 to which the anchor is attached. For transport calculations, the planar conformations of the  
46  
47 molecules were considered, and the gold leads were attached perpendicularly to the plane of  
48  
49 the molecules as discussed in the Methods section. Examples of transmission curves for a  
50  
51 selection of molecules are shown in Figure 2.  
52  
53  
54  
55  
56  
57  
58  
59  
60

1  
2  
3 The circuit formulae are first verified by calculating the room temperature conductance and  
4 thermopower, using the DFT predicted Fermi energies for all molecules. To demonstrate the  
5 circuit rule for conductance, we separately computed the electrical conductances ( $G_{XBY}$ ,  
6  $G_{XBX}$ ,  $G_{YBY}$ ) and Seebeck coefficients ( $S_{XBY}$ ,  $S_{XBX}$ ,  $S_{YBY}$ ) of the individual molecules and  
7 then plotted the square root of the product  $\sqrt{G_{XBX}G_{YBY}}$  versus  $G_{XBY}$ . In Figure 3a, the small  
8 scatter about a straight line demonstrates that in the majority of the cases the circuit rule gives  
9 an accurate prediction for the conductance. To demonstrate the circuit rule for thermopower,  
10 we separately computed the Seebeck coefficients ( $S_{XBY}$ ,  $S_{XBX}$ ,  $S_{YBY}$ ) and then plotted the  
11 average  $(S_{XBX} + S_{YBY})/2$  versus  $S_{XBY}$ , as shown in Figure 3b. This remarkable result means  
12 that from measurements of the conductances  $G_{XBX}$ ,  $G_{YBY}$  it is possible to predict the  
13 conductance  $G_{XBY}$  and similarly for the Seebeck coefficients.  
14  
15  
16  
17  
18  
19  
20  
21  
22  
23  
24  
25  
26  
27

28 We now discuss the sources of deviations from the circuit rule predictions. The inset of  
29 Figure 3a, shows that in a number of cases a slight systematic deviation can be observed. The  
30 origin of these deviations is illustrated by Figure 2, which shows several different  
31 transmission coefficient curves of the X-D<sub>1</sub>-Y type molecules. These show that if the  
32 resonances of the two symmetric molecules are close to each other, then the circuit rule is  
33 accurate over almost the whole of HOMO-LUMO gap; for example in Figures 2a,b, the  
34 dashed purple curves compare well with the black curves. In these cases  $V_X g_X V_X^\dagger \approx V_Y^\dagger g_Y V_Y$ ,  
35 therefore even if  $B_B$  depends strongly on the self energy terms, both sides of the eq. (3)  
36 follow the same energy dependence. On the other hand, if the location of the resonances of  
37 X-B-X and Y-B-Y differ significantly (from Figure 2c to 2h), the error in circuit rule for the  
38 transmission coefficient is large. In particular cases, when transport through one anchor (such  
39 as X=NH<sub>2</sub>) is HOMO dominated, whereas the other anchor (such as Y=Py) is LUMO  
40  
41  
42  
43  
44  
45  
46  
47  
48  
49  
50  
51  
52  
53  
54  
55  
56  
57  
58  
59  
60

1  
2  
3 dominated, but their HOMO-LUMO gaps are similar, then the two self energy terms  $V_X g_X V_X^\dagger$   
4  
5 and  $V_Y^\dagger g_Y V_Y$  are expected to be very different. Such examples can be seen in Figures 2g,h.  
6  
7

8  
9 We also note that the errors in circuit rule predictions for the thermopower are not necessarily  
10 correlated with those of the conductance. While the magnitude of transmission coefficients is  
11 inaccurate, the slope of the transmission curve of the X-D<sub>1</sub>-Y in the log plot in Figure 2g,h  
12 (black curve) remains comparable with the slope of the ones obtained with the circuit rule  
13 (dashed purple). In general,  $\Sigma$  is the smallest and the circuit rule is most accurate when the  
14 Fermi energy is furthest from both the HOMO and LUMO resonances. We note that the DFT  
15 calculations typically significantly underestimate the HOMO-LUMO gap<sup>33-35</sup>, therefore for  
16 realistic electronic structures the circuit rule may applicable even more accurately than shown  
17 in Figure 2 and Figure 3. Other possibilities, that may hinder the accuracy of the circuit rules  
18 for realistic conductances, are thermal fluctuations of the molecular conformation and the  
19 experimental distributions of junction geometries<sup>36</sup>.  
20  
21  
22  
23  
24  
25  
26  
27  
28  
29  
30  
31  
32

33  
34 To facilitate the utilisation of the above circuit rules for single-molecule-junction materials  
35 discovery, we note that they are a consequence of the fact that the transmission coefficients  
36  $T_{XBY}$  can be factorized into a product of the kind  $A_X B_B A_Y$ , where  $A_X$  and  $A_Y$  do not depend  
37 on B, but  $B_B$  may depend on X and Y. Nevertheless when the Fermi energy is located in the  
38 valley of the HOMO-LUMO gap it is possible that  $\Sigma$  is negligible and therefore  $B_B$  depends  
39 only on connectivity and is independent of the choice of the anchor groups. Typically if this  
40 is the case, the transmission coefficients can be factorized to independent factors of anchors  
41 and backbones, and these factors are transferable between different molecules. In other word,  
42 the logarithm of the conductance and the thermopower are sums of transferable factors. To  
43 verify this factorizability, we now assume that computed logarithmic conductance values and  
44 thermopower values can be written  
45  
46  
47  
48  
49  
50  
51  
52  
53  
54  
55  
56  
57  
58  
59  
60



$$\log_{10} \frac{G_{\text{XBY}}}{G_0} = a_X + b_B + a_Y \quad (6)$$

$$\frac{S_{\text{XBY}}}{k_B/e} = a'_X + b'_B + a'_Y \quad (7)$$

where the factors  $a_X, b_B, a_Y, a'_X, b'_B, a'_Y$  are independent and transferable. To obtain these parameters, we minimize numerically the function  $F = \sum_B^{\text{Backbones}} \sum_X^{\text{Anchors}} \sum_{Y \geq X}^{\text{Anchors}} \left( a_X + b_B + a_Y - \log_{10} \frac{G_{\text{XBY}}}{G_0} \right)^2$ , where the  $G_{\text{XBY}}$  values are the DFT-computed conductance values (see Methods section). We note that the separation between the anchor and backbone terms is arbitrary, therefore we set the backbone term of X-RR-Y type molecules to zero, i.e. we choose  $b_{\text{RR}} = 0$ , and in this calculation we choose the molecules in Figure 1a only. With this choice the  $a_X$  terms parametrize the anchoring structures shown in Figure 1a and Table 1, that is the anchor plus the aromatic ring. Consequently the  $b_B$  terms parametrize the backbone, that is the inner part of the molecules between the aromatic rings in Figure 1a. From  $n_A=5$  different anchors and  $n_B=12$  different backbones, this procedure yields 5  $a_X$  parameters and 12  $b_B$  parameters, from which we can reproduce the logarithmic conductance of  $n_A(n_A+1)n_B/2=180$  molecules. Similarly, the same minimizing procedure is used to obtain the thermopower parameters  $a'_X$  and  $b'_B$ . Table 1 shows the anchor and backbone parameters obtained using the above minimizing procedure. To demonstrate that they can be used to predict conductances and thermopowers, Figure 4a shows a comparison between the sum  $a_X + b_B + a_Y$ , and the conductance  $G_{\text{XBY}}$  while Figure 4b compares  $a'_X + b'_B + a'_Y$  with  $S_{\text{XBY}}$ . In Figure 4a, for each molecule, for the DFT computed conductance value  $G_{\text{XBY}}$  on the horizontal axis, we plotted the corresponding  $10^{a_X+b_B+a_Y}G_0$  value marked by a red cross. The fact that the majority of the red crosses are close to the diagonal black line shows that the 5  $a_X$  parameters and 12  $b_B$  parameters in Table 1 can reproduce the logarithmic conductance of the 180 molecules in figure 1a accurately. In essence, by minimizing the function  $F$  with

1  
2  
3 respect to the 5  $a_X$  parameters and 12  $b_B$  parameters, we obtain their optimal value which  
4  
5 holds the information of the conductance values of the 180 molecules. This is possible only  
6  
7 because the conductance can be factorized with good accuracy according to eq. (3) and  
8  
9 therefore the 180 molecular conductances are not independent. Similarly, in Figure 4b, for  
10  
11 each molecule, for the DFT computed thermopower value  $S_{XBY}$  on the horizontal axis, we  
12  
13 plotted the corresponding  $(a'_X + b'_B + a'_Y)S_0$  value marked by a red x. It is interesting to  
14  
15 note that for the conductance, the values of anchor parameter  $a_X$  in Table 1 vary less than the  
16  
17 values of the backbone parameters  $b_B$ . This is in contrast with the thermopower, for which  
18  
19 the magnitudes of the anchor parameters  $a'_X$  vary more than the magnitudes of the backbone  
20  
21 parameters  $b'_B$ , which suggests that the anchor may play a more dominant role in controlling  
22  
23 the thermopower than the conductance.  
24  
25  
26

27  
28 Having demonstrated the validity of the circuit rules, within a consistent set of DFT-based  
29  
30 calculations, we now discuss how they can be used experimentally for real-world discovery  
31  
32 of single-molecule junction properties. Although DFT is widely used for analysing electron  
33  
34 transport in single molecule junctions, it is at best a qualitative theory and therefore for  
35  
36 accurate utilisation of the rules, the parameters  $a_X, b_B, a_Y$  and  $a'_X, b'_B, a'_Y$  should be  
37  
38 determined experimentally. In a typical break junction experiment, the measured value of  
39  
40  $G_{XBY}$  varies markedly from measurement to measurement, because of variability in the  
41  
42 atomic arrangement of the electrodes and in the electrode-anchor group binding geometry.  
43  
44 Consequently many (often thousands) of conductance measurements are made and  
45  
46 histograms of the logarithmic conductance  $g_{XBY} = \log_{10} G_{XBY}/G_0$  are constructed. If  $\bar{g}_{XBY}$   
47  
48 is the most probable value of such a histogram, then the experimentally-quoted value is  
49  
50  $\bar{G}_{XBY}/G_0 = 10^{\bar{g}_{XBY}}$ . This variability is reflected in the anchor parameters  $a_X, a_Y$ . Therefore  
51  
52 when applying the circuit rule to such experiments, it should be applied in a statistical sense.  
53  
54  
55  
56  
57  
58  
59  
60

1  
2  
3 If the most probable values of  $a_X, a_Y$  are  $\bar{a}_X, \bar{a}_Y$ , then the most probable value of  $\log_{10} \frac{G_{XBY}}{G_0}$  is  
4  
5  
6  $\bar{g}_{XBY} = \bar{a}_X + b_B + \bar{a}_Y$ . Conversely, when the fitting procedure of equation (5) in ‘Methods’ is  
7  
8 carried out using experimentally-quoted values, the resulting parameters are  $\bar{a}_X, b_B, \bar{a}_Y$ , rather  
9  
10 than  $a_X, b_B, a_Y$ . This is another reason why it is unsafe to use DFT values to make  
11  
12 quantitative predictions, because it is usually much too expensive to simulate conductance  
13  
14 histograms and therefore typically conductances of only a few anchoring configurations are  
15  
16 reported.

17  
18  
19 At present we are aware of only one set of measurements on both asymmetric (X-B-Y) and  
20  
21 symmetric (X-B-X and Y-B-Y) molecules with the same backbone. In ref <sup>37</sup> the measured  
22  
23 conductance values of molecules S-R-S, NH<sub>2</sub>-R-NH<sub>2</sub> are found to be  $0.012G_0, 0.005G_0$   
24  
25 respectively and for the asymmetric NH<sub>2</sub>-R-S molecule two conductance values  $0.006G_0$  and  
26  
27  $0.009G_0$  were reported. The circuit rule gives  $G/G_0 = 0.008$ , which compares well with both  
28  
29 of the measured values, thereby providing a direct experimental verification of the circuit  
30  
31 rule. To illustrate how the circuit rules can be used to predict experimental conductances for  
32  
33 future molecules from measured values of molecules available in the literature, we make use  
34  
35 of the above factorisation procedure. To perform the fitting, we collected measured  
36  
37 conductances for 19 different molecules from the literature <sup>20, 25, 31, 38-40</sup> and used these to  
38  
39 characterize 5 anchors and 5 backbones. In Table 2 the anchor and backbone parameters are  
40  
41 listed characterized with the experimental conductances. The parameters obtained from the  
42  
43 experimental values are smaller than the theoretical values, as expected, due to the DFT’s  
44  
45 systematic errors with underestimating the HOMO-LUMO gap<sup>35, 41</sup> and the neglect of  
46  
47 environmental and thermal effects in the calculations<sup>36</sup>. Figure 4a and Table 3 show that the  
48  
49 characterisation can reproduce the conductance of the 19 different molecules with good  
50  
51 accuracy (marked with green triangles). The selection covers the typical experimental range  
52  
53 of conductances from  $10^{-2}G_0$  to  $10^{-6}G_0$ . Usually the short molecules with higher conductance,  
54  
55  
56  
57  
58  
59  
60

1  
2  
3 due to the snap back effect in the break-junction methods, are difficult to measure reliably.  
4  
5 The longer molecules with lower conductances (below  $10^{-6} G_0$ ), due to the instrumental  
6  
7 sensitivity, are also difficult to measure. The X-T<sub>n</sub>-X type molecules are from ref<sup>40</sup>, where X  
8  
9 = Py, NH<sub>2</sub>, S, BT and CN, and n=1,2 and 4, but varies for different X because not all  
10  
11 molecules could be synthesized. The conductances for the Py-OPE-Py and Py-OPE(Meta)-  
12  
13 Py type molecules are from ref<sup>20</sup> (Py-OPE(Meta)-Py denotes pmp), for the molecule NH<sub>2</sub>-  
14  
15 OPE-NH<sub>2</sub> is from ref<sup>39</sup> and S-OPE-S molecule is from ref<sup>26</sup>. From ref<sup>29</sup> we obtained the  
16  
17 conductance of NH<sub>2</sub>-RR-NH<sub>2</sub> and from ref<sup>31</sup> Py-RR-Py. The precise conductance values used  
18  
19 in the calculations are quoted in Table 3. Finally we note that in Figure 4a, the green  
20  
21 triangles, and Table 2, 3 and 4 are based on experimental conductance values, which  
22  
23 naturally includes the effect of fluctuations. The fact that the green triangles are close to the  
24  
25 diagonal demonstrates that the circuit rule indeed applies to 19 different experimentally-  
26  
27 quoted most-probable conductances.  
28  
29  
30  
31

32  
33 In conclusion, we have demonstrated that for a large variety of molecules of the type X-B-Y  
34  
35 with different backbones B and anchors X,Y, the molecular conductance and thermopower of  
36  
37 asymmetric molecules can be obtained as geometric and algebraic averages of the zero-bias  
38  
39 conductances and thermopowers of their symmetric counterparts respectively. At a  
40  
41 fundamental level, a requirement for the validity of this ‘circuit rule’ is that the parts X, B  
42  
43 and Y should be weakly coupled, so that multiple scattering effects contained in the self-  
44  
45 energy  $\Sigma$  in equation (1) can be neglected. This also requires that the Fermi energy should be  
46  
47 located within the HOMO-LUMO gap of the molecules and therefore transport should be  
48  
49 ‘off-resonance’ and take place via coherent tunnelling. The validity of this circuit rule is  
50  
51 demonstrated through DFT calculations on 193 molecules, which confirms that the rule  
52  
53 applies to molecules exhibiting off-resonance transport. In our experience of comparing  
54  
55 theory with measurements of single-molecule electron transport, we have found that in  
56  
57  
58  
59  
60

1  
2  
3 almost all cases, unless an electrostatic or electrochemical gate is applied, transport does not  
4  
5 take place near resonances and therefore the rule can be expected to have wide applicability.  
6  
7 The derivation of the rule assumes that transport takes place via coherent tunneling and that  
8  
9 inelastic effects are negligible. Experiment demonstrates that the length scale for the onset of  
10  
11 significant inelastic scattering at room temperature can be of order  $3\text{nm}^{19, 42}$ . All the  
12  
13 molecules in our study are shorter than this length. Furthermore comparison with 19  
14  
15 experimental molecular conductance values from the literature, originating from different  
16  
17 laboratories shows that the circuit rules can be applied successfully at room temperature.  
18  
19 Finally we note that as demonstrated in refs<sup>43, 44</sup> the backbone contribution  $B_B$  (see eq. (2))  
20  
21 depends on the points of contact  $k, l$  of the anchors to the backbone and therefore the circuit  
22  
23 rule should be applied only to families of molecules containing backbones with the same  
24  
25 connectivity to the anchors or equivalently, backbones with different connectivities should be  
26  
27 treated as distinct entities, which means for example that a meta-connected backbone is  
28  
29 distinct from a para-connected backbone as values of  $b_B$  of OPE and OPE(meta) show in  
30  
31 Table 2.  
32  
33  
34  
35  
36

37 For a workable thermoelectric device one needs to increase both the Seebeck coefficient  $S$   
38  
39 and the electrical conductance  $G$  and simultaneously minimise the thermal conductance. The  
40  
41 proposed circuit rule addresses the first two challenges by predicting  $S$  and  $G$  of hitherto  
42  
43 unsynthesized molecules, thereby avoiding unnecessary synthetic effort. The rule also  
44  
45 provides new insight and chemical intuition by organising a large body of information. The  
46  
47 utility of the rule for ‘materials discovery’ derives from the potential translation of single-  
48  
49 molecule functionality into thin molecular films, formed from a monolayer of molecules is  
50  
51 sandwiched between a planar bottom electrode and a planar top electrode, in which the  
52  
53 current/heat flows through the molecules from the bottom to the top electrode. The question  
54  
55 of how single-molecule properties translate into thin films is non-trivial and beyond the scope  
56  
57  
58  
59  
60

1  
2  
3 of this paper. However knowledge of transport properties at the single molecule level will  
4  
5 surely inform our understanding of such thin-film materials.  
6

7 For other properties, the rules can be used to obtain inequalities. For example, they imply  
8  
9 that if  $S_{XX}$  and  $S_{YY}$  have the same sign then the powerfactor  $P_{XY} = G_{XY}S_{XY}^2$  is bounded by the  
10  
11 power factors of the symmetric molecules, that is  $P_{YY} \leq P_{XY} \leq P_{XX}$  and if  $S_{XX}$  and  $S_{YY}$  have  
12  
13 opposite sign, the powerfactor will be diminished significantly. To aid utilisation of the rules  
14  
15 for the discovery of new junction properties, we also demonstrated that conductances and  
16  
17 thermopowers can be characterized by transferable anchor and backbone parameters. Such  
18  
19 characterization can be used to identify optimally functioning molecular devices for future  
20  
21 synthesis. The accuracy of this characterization was demonstrated using experimental  
22  
23 conductances of 19 different molecules from the literature.  
24  
25  
26

27  
28 **Methods.** In order to demonstrate computationally the circuit formulas, we performed DFT  
29  
30 based electron transport calculations on systematically constructed gold-molecule-gold  
31  
32 systems. All together 193 molecules were constructed with attached gold pyramids as  
33  
34 electrodes, with anchors and backbones showed in Figures 1a,b,c. To consistently attach the  
35  
36 pyramids to the molecules with many different backbones and anchors, we first prepared a  
37  
38 relaxed molecular geometry with their planar and extended conformations. The relaxation  
39  
40 was performed with MOPAC2012 RHF method and PM7 parameter-set<sup>45</sup> with constraints  
41  
42 that kept the molecular conformations planar. During the relaxation, the non-hydrogen atoms  
43  
44 were allowed to move only in the molecular plane and only the hydrogen atoms were allowed  
45  
46 to move away from the molecular plane. The initial conformation for the relaxation was  
47  
48 linear extended where the anchors are at the two far ends of the molecule modelling a  
49  
50 possible conformation within an break-junction experiment (shown in Figure 5a) when a  
51  
52 typical conductance plateau is recorded<sup>27, 46</sup>. This is typically occurring when the gap  
53  
54 between the electrodes is slightly less than the molecular length, illustrated in Figure 5a. In  
55  
56  
57  
58  
59  
60

the case of thiol, the sulphur was capped with a hydrogen atom for the relaxation, then after the relaxation the hydrogen atom from the sulphur was removed. We performed relaxations with SIESTA<sup>47</sup> DFT code (force tolerance = 0.01, GGA, DZP) as well for a few molecules and found that planar conformations are usually stable, with significant exceptions of X-RR-Y type molecules, where the aromatic rings are twisted away from each other. Since our investigation focuses on the electronic structures, we consistently kept the all structures planar. For the planar molecular structures a 35-atom 111 directed gold pyramid was attached to the anchoring atoms (S and N) perpendicularly to the molecular plane. The apex gold atom-anchor atom distance was set 2.1Å for the Py, CN anchors, 2.3Å for the NH<sub>2</sub> and BT and 2.35Å for the thiol anchor. This setup allowed consistent systematic comparisons between molecules with different backbones and anchors. The electronic transport calculations were performed by first obtaining the Hamiltonian of the isolated Au-molecule-Au structure by SIESTA, DZP basis set and GGA-PBE exchange-correlation potential parameterization. Then the obtained Hamiltonian was used in GOLLUM<sup>48</sup>, with wide-band approximation to calculate the transmission coefficients, the room temperature conductance and the room temperature thermopower with the DFT computed Fermi energy. The wide-band lead was attached to the two outer layers of the gold pyramid with  $\Gamma = 4.0eV$  coupling<sup>49</sup>. The anchor and backbone parameters were determined by minimizing numerically the function

$$F = \sum_B^{\text{Backbones}} \sum_X^{\text{Anchors}} \sum_{Y \geq X}^{\text{Anchors}} \left( a_X + b_B + a_Y - \log_{10} \frac{G_{XBY}}{G_0} \right)^2 \quad (5)$$

with respect to the various  $a_X, b_B$  parameters with the constraint  $b_{RR} = 0$ , using Broyden-Fletcher-Goldfarb-Shanno (BFGS) method, where 'Backbones' and 'Anchors' are in figure

1  
2  
3 1a,  $G_{XBY}$  is the DFT-computed conductance value and  $Y \geq X$  denotes the exclusion of the  
4  
5 double counting the same molecule.  
6  
7

8 FIGURES  
9

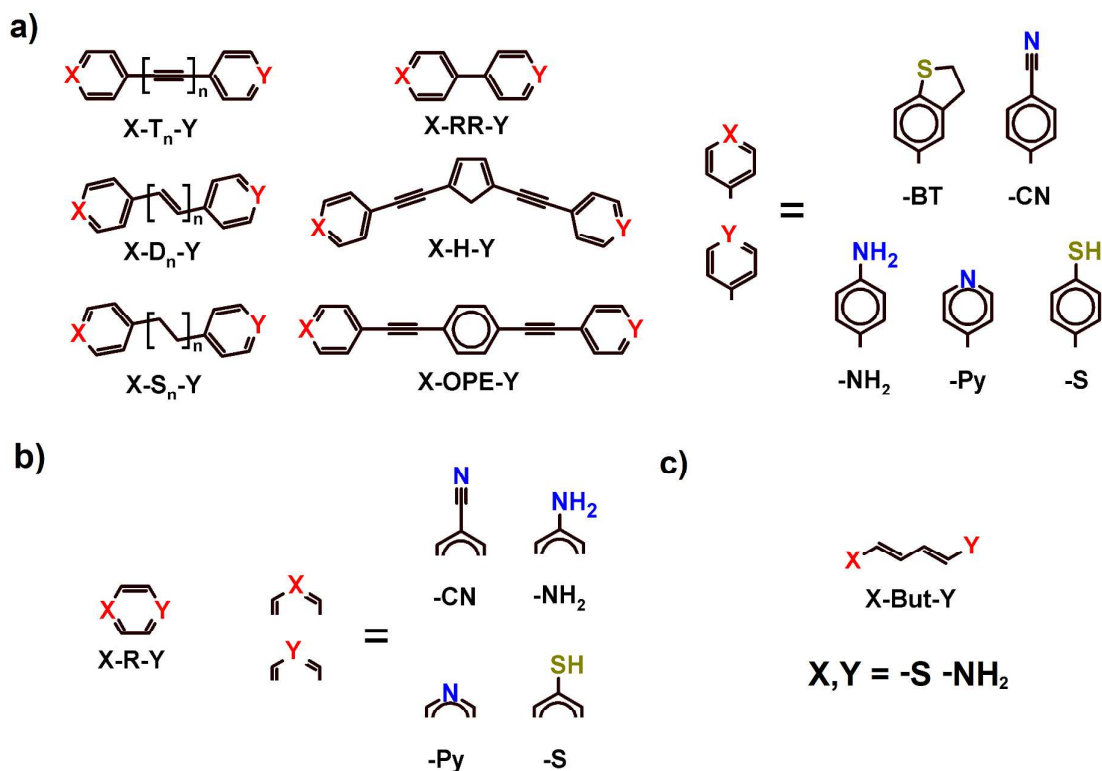


Figure 1. The 193 combinations of backbones and anchors used to obtain figure 2. a) The left column shows 3 alkanes, 3 alkenes and 3 alkynes (where  $n=1,2,3$ ) and the second-from-left column shows 3 other backbones. (ie a total of 12 backbones). The right panel shows 5 anchors cyano (CN), pyridil (Py), dihidrbenzothiol (BT), amine ( $NH_2$ ) and thiol(S). These combine to yield  $12 \times 5$  symmetric molecules and  $12 \times 5 \times 4 / 2 = 120$  asymmetric molecules (ie 180 molecules in total). b) Molecules with a single ring as the backbone and four kinds of anchors: in total there are 4 symmetric and 6 asymmetric variants of these (ie 10 in total). c) shows a single butadiene chain with two kinds of anchors: in total there is one symmetric and



two asymmetric versions of this. All of the molecular geometries are shown in the SI in Figures S1-S14.

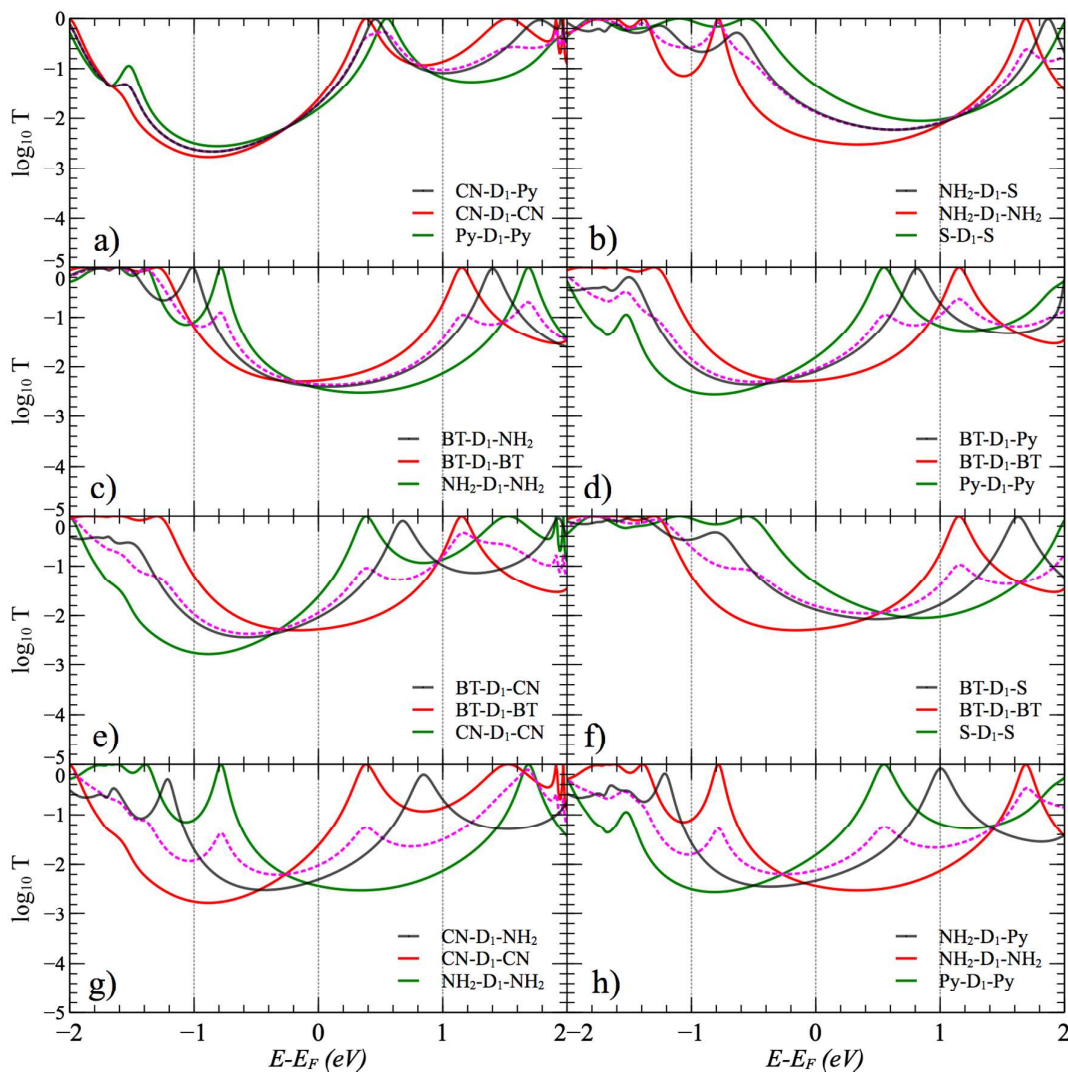


Figure 2. Transmission coefficients for symmetric and asymmetric molecules  $X-D_1-X$ ,  $Y-D_1-Y$  and  $X-D_1-Y$ . The dashed pink curves show the circuit rule predictions for  $X-D_1-Y$ . Choices of  $X$ ,  $Y$  are: (a) CN, Py (b)  $NH_2$ , S (c) BT,  $NH_2$  (d) BT, Py (e) BT, CN (f) BT, S (g) CN,  $NH_2$  (h) Py,  $NH_2$ . Additional transmission coefficient curves are shown in the SI in Figures S15-S28.

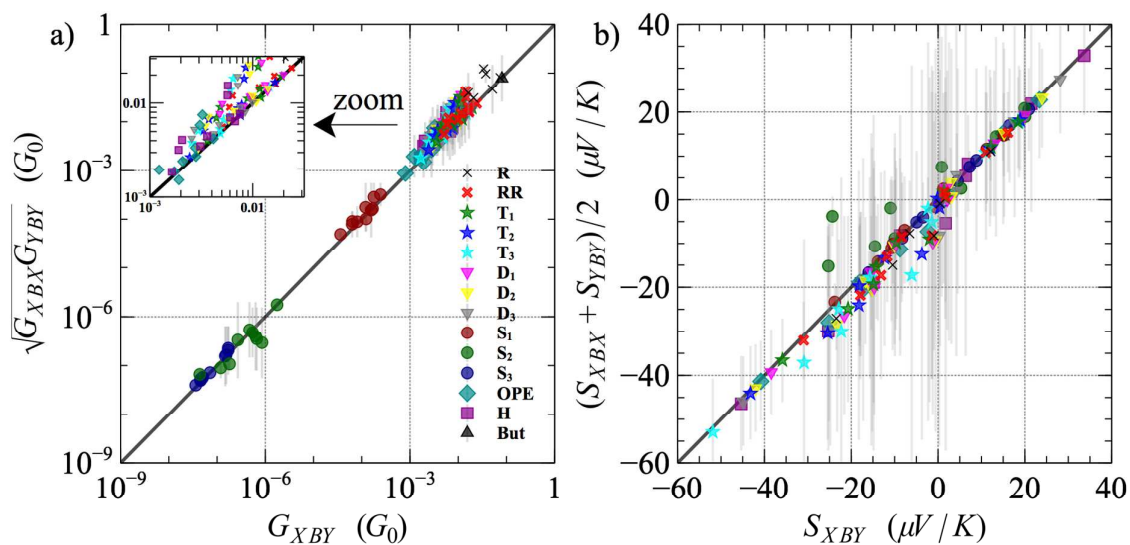


Figure 3. a) Comparison between the conductances  $G_{XBY}$  and the geometric means  $(G_{XBx}G_{YBY})^{1/2}$ . b) Comparison between the thermopowers  $S_{XBY}$  and the arithmetic means  $(S_{XBx} + S_{YBY})/2$ . The top and bottom ends of the vertical grey lines show the values for the symmetric molecules used in the circuit rules. The different colours and markers indicate the various molecular backbones. The notation in the legend is as follows the backbone labelling in Figure 1.

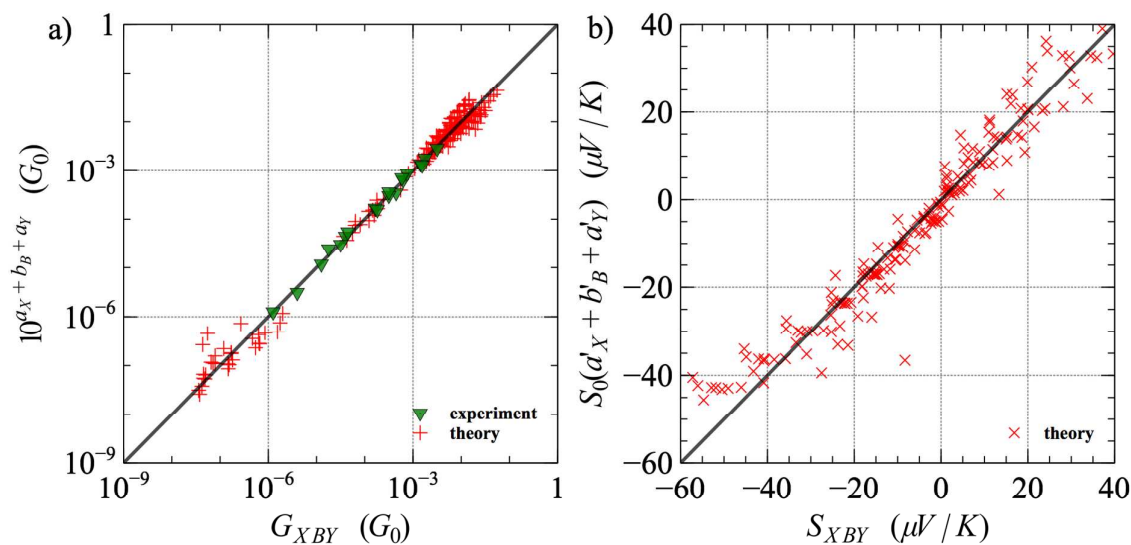


Figure 4. Factorized conductance and thermopower approximations are plotted against the DFT computed values (red markers) and experimental values (green triangles). In panel a), for each DFT-computed conductance  $G_{XBY}$ , a red cross marks the corresponding  $10^{a_X + b_B + a_Y} G_0$  value. In panel b) for each DFT-computed thermopower  $S_{XBY}$ , a red cross marks the corresponding  $(a'_X + b'_B + a'_Y) S_0$  value. In both cases the  $a_X, a'_X$  parameters and  $b_B, b'_B$  parameters are taken from Table 1. The green triangles in panel a) show the factorization of a selection of experimental conductances from the literature, quoted in Table 3. For each experimental conductance  $G_{XBY}$  the green triangle marks the corresponding  $10^{a_X + b_B + a_Y} G_0$  value, where the  $a_X$  parameters and  $b_B$  parameters are taken from Table 2.  $G_0 = 2e^2/h$ .  $S_0 = k_B/e$ .

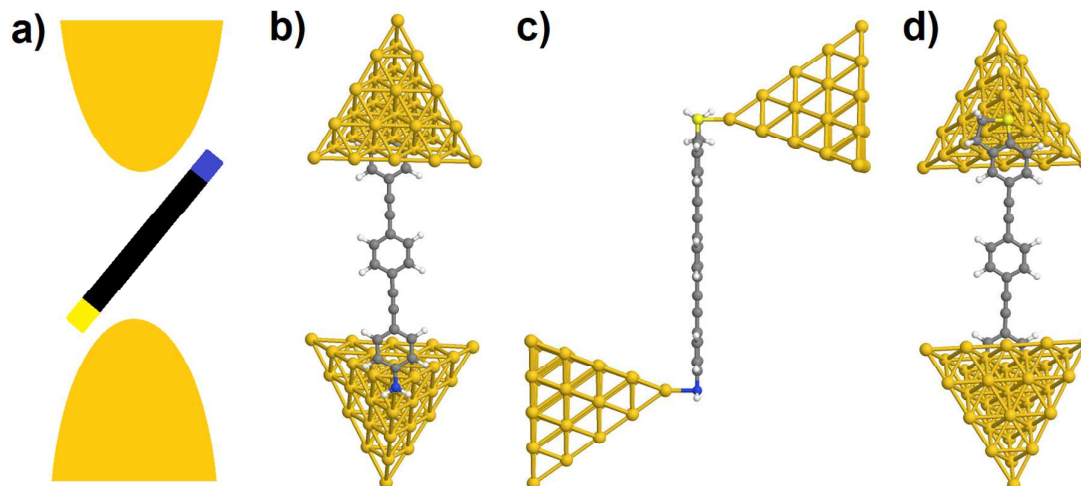


Figure 5. a) Molecule arrangement in break-junction experiment. b),c),d) Three views of the same junction. Top, side and bottom views, respectively, of the model junction geometry of a particular case (BT-OPE-NH<sub>2</sub>) for systematic comparisons.

## TABLES

Table 1 Anchor and backbone parameters obtained by fitting eqs. 3 and 4 to the DFT-computed room temperature conductances ( $\log_{10}(G/G_0)$ ) and thermopowers ( $Se/k_B$ ) respectively

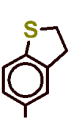




Anchor X with rings		 -BT	 -CN	 -NH <sub>2</sub>	 -Py	 -S
$a_X$		-1.12	-0.89	-1.20	-0.87	-0.68
$a'_X$		-0.02	-0.24	0.06	-0.17	0.19
Backbones B	RR	T <sub>1</sub>	T <sub>2</sub>	T <sub>3</sub>	OPE	H
$b_B$	0.00	-0.12	-0.25	-0.38	-0.73	-0.46
$b'_B$	0.00	-0.01	-0.05	-0.09	-0.02	0.01
Backbones B	D <sub>1</sub>	D <sub>2</sub>	D <sub>3</sub>	S <sub>1</sub>	S <sub>2</sub>	S <sub>3</sub>
$b_B$	-0.09	-0.22	-0.35	-2.04	-4.57	-5.19
$b'_B$	-0.01	-0.01	-0.01	0.03	0.06	0.10

Table 2 Anchor and backbone parameters obtained by fitting eq. 3 to the experimental room temperature conductance ( $\log_{10}(G/G_0)$ ). For the  $n_A=5$  anchor and  $n_B=6$  backbone, the parameters give the

conductance of  $n_A(n_A+1)n_B/2=90$  molecules in the form of  $G_{XBY} = 10^{a_X+b_B+a_Y}G_0$ .<sup>(a)</sup> an example for this backbone is 'pmp' from ref<sup>20</sup>.

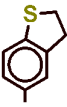




Anchor X with rigins						
		-BT	-CN	-NH <sub>2</sub>	-Py	-S
$a_X$ (from experiments)	-	-1.12	-2.15	-1.44	-1.58	-1.22
Backbones B	RR	T <sub>1</sub>	T <sub>2</sub>	T <sub>4</sub>	OPE	OPE(meta) <sup>(a)</sup>
$b_B$ (from experiments)	0.00	-0.31	-0.63	-1.20	-1.37	-2.75

Table 3 Comparison between experimental conductances and the computed conductances from equ. 3, using the fitted anchor and backbone parameters shown in table 2. Experimental values are taken from<sup>(a)</sup> from ref<sup>40</sup> by averaging STM-BJ and MCBJ values, <sup>(b)</sup> from ref<sup>31</sup>, <sup>(c)</sup> from ref<sup>20</sup>, <sup>(d)</sup> from ref<sup>26</sup>, <sup>(e)</sup> from ref<sup>39</sup>, <sup>(f)</sup> from ref<sup>29</sup>.

Molecule X B Y	Experimental $\log_{10} \frac{G}{G_0}$	$a_X + b_B + a_Y$	Molecule X B Y	Experimental $\log_{10} \frac{G}{G_0}$	$a_X + b_B + a_Y$
Py T <sub>1</sub> Py	-3.35 <sup>(a)</sup>	-3.47	CN T <sub>1</sub> CN	-4.75 <sup>(a)</sup>	-4.61
Py T <sub>2</sub> Py	-3.78 <sup>(a)</sup>	-3.79	CN T <sub>2</sub> CN	-4.9 <sup>(a)</sup>	-4.93
Py T <sub>4</sub> Py	-4.4 <sup>(a)</sup>	-4.36	CN T <sub>4</sub> CN	-5.4 <sup>(a)</sup>	-5.50
NH <sub>2</sub> T <sub>1</sub> NH <sub>2</sub>	-3.205 <sup>(a)</sup>	-3.19	S T <sub>1</sub> S	-2.75 <sup>(a)</sup>	-2.75
NH <sub>2</sub> T <sub>2</sub> NH <sub>2</sub>	-3.5 <sup>(a)</sup>	-3.51	S T <sub>2</sub> S	-3.12 <sup>(a)</sup>	-3.07
BT T <sub>1</sub> BT	-2.5 <sup>(a)</sup>	-2.55	Py OPE Py	-4.5 <sup>(c)</sup>	-4.53
BT T <sub>2</sub> BT	-2.845 <sup>(a)</sup>	-2.87	S OPE S	-3.74 <sup>(d)</sup>	-3.81
BT T <sub>4</sub> BT	-3.5 <sup>(a)</sup>	-3.44	NH <sub>2</sub> OPE NH <sub>2</sub>	-4.35 <sup>(e)</sup>	-4.25
Py RR Py	-3.23 <sup>(b)</sup>	-3.15	Py OPE(meta) Py (pmp) <sup>(e)</sup>	-5.9 <sup>(c)</sup>	-5.91
NH <sub>2</sub> RR NH <sub>2</sub>	-2.81 <sup>(f)</sup>	-2.89			

**Table 4 Conductance predictions for a few new molecules based on Table 2. Predictions from Table 2 for all combinations of backbones and anchors are presented in Table S1 of the SI.**

Molecule X B Y	$a_X + b_B + a_Y$ ( $\log_{10}(G/G_0)$ )	Molecule X B Y	$a_X + b_B + a_Y$ ( $\log_{10}(G/G_0)$ )
Py-T <sub>1</sub> -CN	-4.04	Py-OPE-NH <sub>2</sub>	-4.39
Py-T <sub>1</sub> -NH <sub>2</sub>	-3.33	Py-OPE-BT	-4.07
Py-T <sub>1</sub> -BT	-3.01	Py-OPE-S	-4.17
Py-T <sub>1</sub> -S	-3.11	CN-OPE-CN	-5.67
CN-T <sub>1</sub> -NH <sub>2</sub>	-3.90	CN-OPE-NH <sub>2</sub>	-4.96
CN-T <sub>1</sub> -BT	-3.58	CN-OPE-BT	-4.64
CN-T <sub>1</sub> -S	-3.68	CN-OPE-S	-4.74
NH <sub>2</sub> -T <sub>1</sub> -BT	-2.87	NH <sub>2</sub> -OPE-BT	-3.93
NH <sub>2</sub> -T <sub>1</sub> -S	-2.97	NH <sub>2</sub> -OPE-S	-4.03
BT-T <sub>1</sub> -S	-2.65	BT-OPE-BT	-3.61
Py-OPE-CN	-5.10	BT-OPE-S	-3.71

## ASSOCIATED CONTENT

Supporting Information Available: Content includes figures for all molecular geometries and all computed transmission coefficient functions. Theoretical predictions for the conductance of all anchor group/backbone combinations are included in Table S1. This material is available free of charge via internet at <http://pubs.acs.org>.

## AUTHOR INFORMATION

### Corresponding Author

[c.lambert@lancaster.ac.uk](mailto:c.lambert@lancaster.ac.uk); [d.manrique@lancaster.ac.uk](mailto:d.manrique@lancaster.ac.uk);

### Present Addresses

†If an author's address is different than the one given in the affiliation line, this information may be included here.

### Author Contributions

DZM, WH and CJL conceived the research idea. The calculations were performed by DZM and QA and the manuscript has been prepared by DZM, QA and CJL. The manuscript was written through contributions of all authors. All authors have given approval to the final version of the manuscript.

## Notes

The authors declare no competing financial interest.

## ACKNOWLEDGMENTS

This work was generously supported by the UK EPSRC projects EP/N017188/1, EP/M014452/1, the EC FP7 ITN "MOLESCO" project number 606728, and the Higher Education Ministry, Al Qadisiyah University, IRAQ.

## REFERENCES

- (1) Repp, J.; Meyer, G.; Paavilainen, S.; Olsson, F. E.; Persson, M. *Science* **2006**, 312, (5777), 1196-1199.
- (2) Donhauser, Z. J.; Mantooth, B. A.; Kelly, K. F.; Bumm, L. A.; Monnell, J. D.; Stapleton, J. J.; Price Jr., D. W.; Rawlett, A. M.; Allara, D. L.; Tour, J. M.; Weiss, P. S. *Science* **2001**, 292, 2303-2307.
- (3) Wold, D. J.; Haag, R.; Rampi, M. A.; Frisbie, C. D. *J. Phys. Chem. B* **2002**, 106, (11), 2813-2816.
- (4) Fan, F. R. F. *J. Am. Chem. Soc.* **2002**, 124, 5550-5560.
- (5) Widawsky, J. R.; Darancet, P.; Neaton, J. B.; Venkataraman, L. *Nano Lett.* **2012**, 12, (1), 354-358.
- (6) Venkataraman, L.; Klare, J. E.; Nuckolls, C.; Hybertsen, M. S.; Steigerwald, M. L. *Nat.* **2006**, 442, (7105), 904-907.
- (7) Hong, W.; Valkenier, H.; Meszaros, G.; Manrique, D. Z.; Mishchenko, A.; Putz, A.; Garcia, P. M.; Lambert, C. J.; Hummelen, J. C.; Wandlowski, T. *Beilstein J. Nanotechnol.* **2011**, 2, 699-713.
- (8) Seferos, D. S.; Trammell, S. A.; Bazan, G. C.; Kushmerick, J. G. *P. NATL. ACAD. SCI. USA* **2005**, 102, (25), 8821-8825.
- (9) Dadosh, T.; Gordin, Y.; Krahne, R.; Khivrich, I.; Mahalu, D.; Frydman, V.; Sperling, J.; Yacoby, A.; Bar-Joseph, I. *Nat.* **2005**, 436, (7054), 1200-1200.
- (10) Liao, J.; Bernard, L.; Langer, M.; Schonenberger, C.; Calame, M. *Adv. Mater.* **2006**, 18, (18), 2803-2804.
- (11) Reed, M. A.; Zhou, C.; Muller, C. J.; Burgin, T. P.; Tour, J. M. *Science* **1997**, 278, (5336), 252-254.
- (12) Park, J.; Pasupathy, A. N.; Goldsmith, J. I.; Chang, C.; Yaish, Y.; Petta, J. R.; Rinkoski, M.; Sethna, J. P.; Abruña, H. D.; McEuen, P. L. *Nat.* **2002**, 417, (6890), 722-725.
- (13) Osorio, E.; Bjørnholm, T.; Lehn, J.; Ruben, M.; Van der Zant, H. *J. Phys.: Condens. Matter* **2008**, 20, (37), 374121.
- (14) Chen, J.; Reed, M. A.; Rawlett, A. M.; Tour, J. M. *Science* **1999**, 286, 1550-1552.

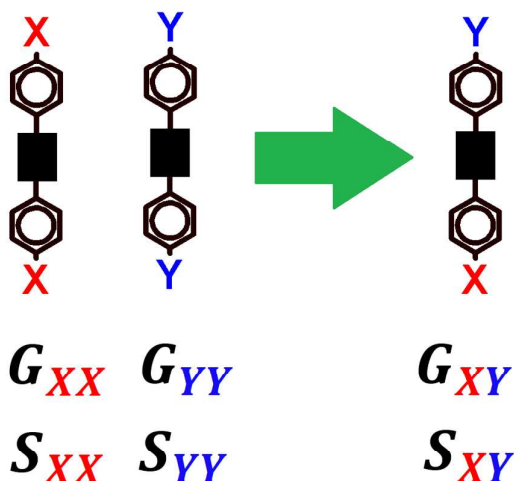


- 1  
2  
3 (15) Aviram, A.; Ratner, M. *Chem. Phys. Lett.* **1974**, *29*, 277-283.
- 4 (16) Finch, C. M.; Sirichantaropass, S.; Bailey, S. W.; Grace, I. M.; García-Suárez, V. M.;  
5 Lambert, C. J. *J. Phys.: Condens. Matter* **2008**, *20*, (2), 022203.
- 6 (17) Peterfalvi, C. G.; Grace, I.; Manrique, D. Z.; Lambert, C. J. *J. Chem. Phys* **2014**, *140*,  
7 (17), 174711.
- 8 (18) Evangeli, C.; Gillemot, K.; Leary, E.; González, M. T.; Rubio-Bollinger, G.; Lambert,  
9 C. J.; Agrait, N. *Nano Lett.* **2013**, *13*, (5), 2141-2145.
- 10 (19) Zhao, X.; Huang, C.; Gulcur, M.; Batsanov, A. S.; Baghernejad, M.; Hong, W.;  
11 Bryce, M. R.; Wandlowski, T. *Chem. Mater.* **2013**, *25*, (21), 4340-4347.
- 12 (20) Manrique, D. Z.; Huang, C.; Baghernejad, M.; Zhao, X.; Al-Owaedi, O. A.; Sadeghi,  
13 H.; Kaliginedi, V.; Hong, W.; Gulcur, M.; Wandlowski, T.; Bryce, M. R.; Lambert, C. J. *Nat.*  
14 *Commun.* **2015**, *6*, 6389A, No. 8.
- 15 (21) Lambert, C. *Chem. Soc. Rev.* **2015**, *44*, (4), 875-888.
- 16 (22) Cuevas, J. C.; Scheer, E., *Molecular electronics: an introduction to theory and*  
17 *experiment. World Scientific: 2010; Vol. 1.*
- 18 (23) Sparks, R.; García-Suárez, V. M.; Manrique, D. Z.; Lambert, C. J. *Phys. Rev. B* **2011**,  
19 *83*, (7), 075437.
- 20 (24) Finch, C. M.; Garcia-Suarez, V. M.; Lambert, C. J. *Phys. Rev. B* **2009**, *79*, (3),  
21 033405.
- 22 (25) Hong, W.; Manrique, D. Z.; Moreno-Garcia, P.; Gulcur, M.; Mishchenko, A.;  
23 Lambert, C. J.; Bryce, M. R.; Wandlowski, T. *J. Am. Chem. Soc.* **2012**, *134*, (4), 2292-2304.
- 24 (26) Kaliginedi, V.; Moreno-García, P.; Valkenier, H.; Hong, W.; García-Suárez, V. M.;  
25 Buitter, P.; Otten, J. L. H.; Hummelen, J. C.; Lambert, C. J.; Wandlowski, T. *J. Am. Chem.*  
26 *Soc.* **2012**, *134*, (11), 5262-5275.
- 27 (27) Yoshida, K.; Pobelov, I. V.; Manrique, D. Z.; Pope, T.; Meszaros, G.; Gulcur, M.;  
28 Bryce, M. R.; Lambert, C. J.; Wandlowski, T. *Sci. Rep.* **2015**, *5*, 9002A, No. 8.
- 29 (28) Mishchenko, A.; Zotti, L. A.; Vonlanthen, D.; Buerkle, M.; Pauly, F.; Carlos Cuevas,  
30 J.; Mayor, M.; Wandlowski, T. *J. Am. Chem. Soc.* **2011**, *133*, (2), 184-187.
- 31 (29) Hybertsen, M. S.; Venkataraman, L.; Klare, J. E.; Cwhalley, A.; Steigerwald, M. L.;  
32 Nuckolls, C. *J. Phys.: Condens. Matter* **2008**, *20*, (37), 374115.
- 33 (30) Quek, S. Y.; Venkataraman, L.; Choi, H. J.; Louie, S. G.; Hybertsen, M. S.; Neaton, J.  
34 B. *Nano Lett.* **2007**, *7*, (11), 3477-3482.
- 35 (31) Quek, S. Y.; Kamenetska, M.; Steigerwald, M. L.; Choi, H. J.; Louie, S. G.;  
36 Hybertsen, M. S.; Neaton, J. B.; Venkataraman, L. *Nat. Nanotechnol.* **2009**, *4*, (4), 230-234.
- 37 (32) Kanthasamy, K.; Pfnuer, H. *Beilstein J. Nanotechnol.* **2015**, *6*, 1690-1697.
- 38 (33) Egger, D. A.; Liu, Z.-F.; Neaton, J. B.; Kronik, L. *Nano Letters* **2015**, *15*, (4), 2448-  
39 2455.
- 40 (34) Jin, C.; Strange, M.; Markussen, T.; Solomon, G. C.; Thygesen, K. S. *J. Chem. Phys.*  
41 **2013**, *139*, (18), 184307.
- 42 (35) Quek, S. Y.; Khoo, K. H. *Acc. Chem. Res.* **2014**, *47*, (11), 3250-3257.
- 43 (36) Berritta, M.; Manrique, D. Z.; Lambert, C. J. *Nanoscale* **2015**, *7*, (3), 1096-1101.
- 44 (37) Wang, K.; Zhou, J.; Hamill, J. M.; Xu, B. *J. Chem. Phys.* **2014**, *141*, (5), 054712.
- 45 (38) Baghernejad, M.; Manrique, D. Z.; Li, C.; Pope, T.; Zhumaev, U.; Pobelov, I.;  
46 Moreno-Garcia, P.; Kaliginedi, V.; Huang, C.; Hong, W.; Lambert, C.; Wandlowski, T.  
47 *Chem. Commun.* **2014**, *50*, (100), 15975-15978.
- 48 (39) Gonzalez, T. M.; Zhao, X.; Manrique, D. Z.; Miguel, D.; Leary, E.; Gulcur, M.;  
49 Batsanov, A. S.; Rubio-Bollinger, G.; Lambert, C. J.; Bryce, M. R.; Agrait, N. *J. Phys.*  
50 *Chem. C* **2014**, *118*, (37), 21655-21662.
- 51  
52  
53  
54  
55  
56  
57  
58  
59  
60



- (40) Moreno-Garcia, P.; Gulcur, M.; Manrique, D. Z.; Pope, T.; Hong, W.; Kaliginedi, V.; Huang, C.; Batsanov, A. S.; Bryce, M. R.; Lambert, C.; Wandlowski, T. *J. Am. Chem. Soc.* **2013**, 135, (33), 12228-12240.
- (41) Kim, T.; Darancet, P.; Widawsky, J. R.; Kotiuga, M.; Quek, S. Y.; Neaton, J. B.; Venkataraman, L. *Nano Lett.* **2014**, 14, (2), 794-798.
- (42) Sedghi, G.; García-Suárez, V. M.; Esdaile, L. J.; Anderson, H. L.; Lambert, C. J.; Martín, S.; Bethell, D.; Higgins, S. J.; Elliott, M.; Bennett, N. *Nat. Nanotechnol.* **2011**, 6, (8), 517-523.
- (43) Sangtarash, S.; Huang, C.; Sadeghi, H.; Sorohhov, G.; Hauser, J. r.; Wandlowski, T.; Hong, W.; Decurtins, S.; Liu, S.-X.; Lambert, C. J. *J. Am. Chem. Soc.* **2015**, 137, (35), 11425-11431.
- (44) Geng, Y.; Sangtarash, S.; Huang, C.; Sadeghi, H.; Fu, Y.; Hong, W.; Wandlowski, T.; Decurtins, S.; Lambert, C. J.; Liu, S.-X. *J. Am. Chem. Soc.* **2015**, 137, (13), 4469-4476.
- (45) Stewart, J. J. P. *J. Mol. Model.* **2013**, 19, (1), 1-32.
- (46) Huang, C. C.; Rudnev, A. V.; Hong, W. J.; Wandlowski, T. *Chem. Soc. Rev.* **2015**, 44, (4), 889-901.
- (47) Soler, J. M.; Artacho, E.; Gale, J. D.; García, A.; Junquera, J.; Ordejón, P.; Sánchez-Portal, D. *J. Phys.: Condens. Matter.* **2002**, 14, (11), 2745.
- (48) Ferrer, J.; Lambert, C. J.; Garcia-Suarez, V. M.; Manrique, D. Z.; Visontai, D.; Oroszlany, L.; Rodriguez-Ferradas, R.; Grace, I.; Bailey, S. W. D.; Gillemot, K.; Sadeghi, H.; Algharagholi, L. A. *New J. Phys.* **2014**, 16, 093029.
- (49) Verzijl, C. J. O.; Seldenthuis, J. S.; Thijssen, J. M. *J. Chem. Phys.* **2013**, 138, (9), 094102.

## TABLE OF CONTENT GRAPHICS



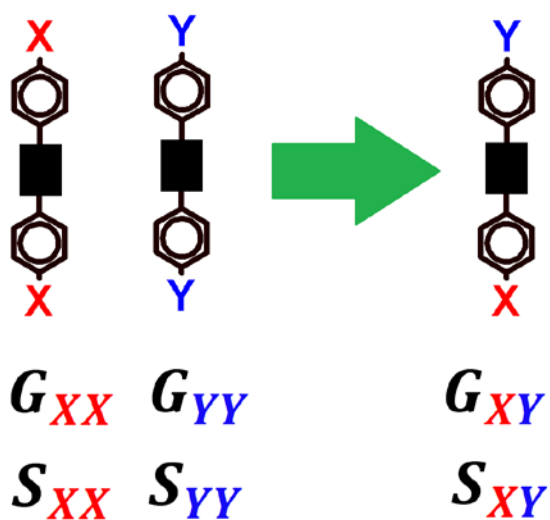
## Conductance

$$G_{XY} = \sqrt{G_{XX}G_{YY}}$$

## Thermopower

$$S_{XY} = \frac{S_{XX} + S_{YY}}{2}$$

## TABLE OF CONTENT GRAPHICS

**Conductance**

$$G_{XY} = \sqrt{G_{XX}G_{YY}}$$

**Thermopower**

$$S_{XY} = \frac{S_{XX} + S_{YY}}{2}$$